terns are suggestive of low-temperature alteration; their higher temperature steps, representing 42 and 20% of the total ^{39}Ar released, would indicate minimal crystallization ages of 64.6 ± 0.4 Ma and 65.2 ± 1.2 Ma. In an addi-tional experiment, four increments in the middle of a rising release spectrum for a 1.0-mg bulk plagioclase analysis, between 800° and 1050°C, representing approximately 25 to 30% of the total ^{39}Ar released, yielded a weighted mean age of the C-1 melt rock, give a weighted mean age of 64.7 ± 0.4 Ma, consistent with the previously discussed results. The variability in release patterns noted here are most likely a result of differential alteration and small-scale inhomogeneity of the sample.

REFERENCES AND NOTES

1. G. T. Penfield and A. Camargo Z., *Soc. Expl. Geophys. Int. Meet.* **51**, 37 (1981).
2. A. R. Hildebrand *et al.*, *Geology* **19**, 867 (1991).
3. G. T. Izett *et al.*, *U.S. Geol. Surv. Open-File Rep. 90-635* (1990), p. 1.
4. H. Sigurdsson *et al.*, *Nature* **349**, 482 (1991).
5. F. J-M. R. Maurrasse and G. Sen, *Science* **252**, 1690 (1991).
6. J. Smit *et al.*, *Geology* **20**, 99 (1992).
7. W. Alvarez *et al.*, *ibid.*, in press.
8. E. López Ramos, *The Gulf of Mexico and the Caribbean*, vol. 3 of *The Ocean Basins and Margins*, A. E. M. Nairn and F. G. Stehli, Eds. (Plenum, New York, 1975), *Geología de México, Univ. Nac. Autón. de México* **269** (1983).
9. G. E. Murray and A. E. Weidie, Jr., in *Field Trip to Peninsula of Yucátan*, A. E. Weidie Jr., Ed., (Guidebook, New Orleans Geological Society, New Orleans, LA, 1967).
10. R. H. Marshall, thesis, University of New Orleans (1974).
11. G. Keller and W. Sliter, as cited in (*2*).
12. Analytical procedures follow A. Deino and R. Potts [*J. Geophys. Res.* **95**, 8453 (1990)], A Deino, L. Tauxe, M. Monaghan, and R. Drake [*J. Geol.* **98**, 567 (1990)], C. C. Swisher III and D. R. Prothero [*Science* **249**, 760 (1990)], and P. R. Renne and A. R. Basu [*ibid.* **253**, 176 (1991)]. The maximum output of the laser during this study was approximately 8 W. Ca and K corrections were determined from laboratory salts: $(^{36}Ar/^{37}Ar)_{Ca} = 2.557 \times 10^{-4} \pm 4.6 \times 10^{-6}$, $(^{39}Ar/^{37}Ar)_{Ca} = 6.608 \times 10^{-4} \pm 2.53 \times 10^{-5}$, and $(^{40}Ar/^{39}Ar)_{K} = 2.4 \times 10^{-3} \pm 7.0 \times 10^{-4}$. J [0.0099585 ± 0.0000058 (± 0.06%)] was based on 20 replicate single crystal analyses of the monitor mineral Fish Canyon (FC) sanidine with an age of 27.84 Ma. Mass discrimination during this study, as determined by replicate air aliquots delivered from an on-line pipette system, was 1.006 ± 0.00015. The Haitian tektites were similarly irradiated for 21 hours (J = 0.017015 ± 0.000016) and for 7 hours (two levels; J = 0.0059649 ± 0.0000096 and 0.0059058 ± 0.00000534) according with procedures and calibrations outlined above and in text. Decay constants are those reccommended by R. H. Steiger and E. Jager [*Earth Planet. Sci. Lett.* **36**, 359 (1977)] and G. B. Dalrymple [*Geology* **7**, 558 (1979)].
13. The age of the FC sanidine adopted in this study (27.84 Ma) is similar to that recommended by G. T. Cebula *et al.* [*Terra Cognita* **6**, 139 (1986)] but slightly modified as a result of in-house intercalibration with MMhb-I with an age of 520.4 ± 1.7 Ma [S. D. Samson and E. C. Alexander, *Chem. Geol. Isot. Geosci. Sect.* **66**, 27 (1987)].
14. The uncertainties associated with the individual incremental apparent ages are 2σ errors, whereas those that accompany the calculated weighted mean ages of the plateau increments and weighted means of the replicate analyses are standard errors (SE) following J. R. Taylor [*An Introduction to Error Analysis* (Oxford Univ. Press, New York, 1982)].
15. Plateau definition basically follows R. J. Fleck *et al.* [*Geochim. Cosmochim. Acta* **41**, 15 (1977)].
16. G. A. Izett, G. B. Dalrymple, L. W. Snee, *Science* **252**, 1539 (1991).
17. C. M. Hall, D. York, and H. Sigurdsson [Eos **72**, 531 (1991)] reported a weighted mean $^{40}Ar/^{39}Ar$ plateau age for the Haitian tektites of 64.75 ± 0.28 Ma; MMhb-I = 517.0 Ma. P. Y. Gillot, C. Jehanno, R. Rocchia, and H. Sigurdsson [*C. R. Acad. Sci.*, **313**, 193 (1991)] reported a K-Ar age for the Haitian tektite of 64.0 ± 0.7 Ma. M. O. McWilliams, A. K. Baksi, and B. F. Bohor [*Eos* **73**, 363 (1992)] reported a slightly older mean $^{40}Ar/^{39}Ar$ age for the Haitian tektites of 64.91 ± 0.12 Ma, Taylor Creek Rhyolite = 27.92.
18. FC sanidine was used as a monitor over MMhb-I, primarily, because of its far superior grain to grain and irradiation to irradiation reproducibility. Izett *et al.* (*16*) indicated that FC sanidine was also used as one of their monitor minerals in the calibration of their age for the Haitian tektites. Using their reported age for FC of 27.55 Ma and our age for FC sanidine of 27.84 Ma, we recalculate the Menlo Park ages for the Haitian tektites as follows: plateau age = 64.38 × (27.84/27.55) = 65.06 Ma and total fusion age = 64.48 × (27.84/27.55) = 65.16 Ma.
19. R. E. Folinsbee, H. Baadsgaard, G. L. Cumming, *Nucl. Geophys.* **1075**, 70 (1963); M. Shafiqullah, R. E. Folinsbee, H. Baadsgaard, H. Cumming, J. F. Lerbekmo, paper presented at the XXII Int. Geol. Congr. New Delhi, part III, section 3 (1964); J. F. Evernden, D. E. Savage, G. H. Curtis, G. T. James, *Am. J. Sci.* **262**, 145 (1964); J. D. Obradovich and W. A. Cobban, *Geol. Assoc. Can. Spec. Pap.* **13**, 31 (1975); H. Baadsgaard and J. F. Lerbekmo, *Can. J. Earth Sci.* **17**, 671 (1980); *ibid.* **20**, 1282 (1983); J. D. Obradovich, *Stratigraphy* **1**, 11 (1984); H. Baadsgaard, J. F. Lerbekmo, I. J. F. McDougall, *Can. J. Earth Sci.* **25**, 1088 (1988); M. O. McWilliams, A. K. Baksi, B. F. Bohor *Eos* **73**, 363 (1992); W. A. Berggren, D. Kent, J. D. Obradovich, C. C. Swisher, in *Eocene-Oligocene Climatic and Biotic Evolution*; D. R. Prothero and W. A. Berggren, Eds. (Princeton Univ. Press, Princeton, NJ, in press).
20. W. Alvarez and F. Asaro, *Sci. Am.* **263**, 78 (October 1990).
21. M. J. Kunk, G. A. Izett, R. A. Haugerud, J. F. Sutter, *Science* **244**, 1565 (1989); J. B. Hartung, M. J. Kunk, R. R. Anderson, *Geol. Soc. Am. Spec. Pap.* **247**, 207 (1990).
22. L. E. Marin *et al.*, *Proc. Lunar Planet. Sci. Conf.* **22**, in press.
23. B. F. Bohor and W. J. Betterton, *ibid.* **20**, 107 (1990); J. Smit *et al.*, *ibid.*, in press.

24. This study was supported by the Institute of Human Origins, National Science Foundation grant EAR 91-05297, National Aeronautics and Space Administration grant NAGW 3008, Petróleos Mexicanos, and the Instituto Mexicano del Petróleo.

10 June 1992; accepted 1 July 1992

Pseudo–Half-Knot Formation with RNA

D. J. Ecker,* T. A. Vickers, T. W. Bruice, S. M. Freier, R. D. Jenison, M. Manoharan, M. Zounes

A pseudo–half-knot can be formed by binding an oligonucleotide asymmetrically to an RNA hairpin loop. This binding motif was used to target the human immunodeficiency virus TAR element, an important viral RNA structure that is the receptor for Tat, the major viral transactivator protein. Oligonucleotides complementary to different halves of the TAR structure bound with greater affinity than molecules designed to bind symmetrically around the hairpin. The pseudo–half-knot–forming oligonucleotides altered the TAR structure so that specific recognition and binding of a Tat-derived peptide was disrupted. This general binding motif may be used to disrupt the structure of regulatory RNA hairpins.

The RNA duplex structure is not favorable for antisense or ribozyme binding. Folded RNA, however, has short single-stranded segments that may be used to initiate antisense hybridization, followed by propagation of the heteroduplex into structured regions (*1*). Structured RNA regions often are recognized by regulatory proteins (*2–5*), and targeting these structures with an antisense oligonucleotide may block binding of a regulatory protein.

The simplest example of RNA secondary structure is a hairpin consisting of a double-stranded stem region and a single-stranded loop. Hybridization to all of the unpaired bases in the loop without disrupting base pairing in the stem would seem an attractive strategy but is sterically impossible. Pseudoknots are naturally occurring RNA structures where hairpin loops are base paired in stable and sterically possible conformations. Single-stranded bases of an RNA hairpin loop create a pseudoknot by pairing with bases adjacent to the hairpin, forming a second stem and loop (Fig. 1) (*6–9*). An RNA pseudoknot contains two coaxially stacked stems and two topologically distinct loops, L1 and L2. L1 crosses the major groove and L2 crosses the minor groove.

When an antisense oligoribonucleotide is hybridized asymmetrically to the loop of a hairpin, the topology of the resulting complex resembles half a pseudoknot. If hybridized to the 3′ side of the loop (Fig. 1A, top path), a structure equivalent to S2 is formed and the looped-out RNA is equivalent to L1. If hybridized to the 5′ side of the

ISIS Pharmaceuticals, 2280 Faraday Avenue, Carlsbad, CA 92008

*To whom correspondence should be addressed.

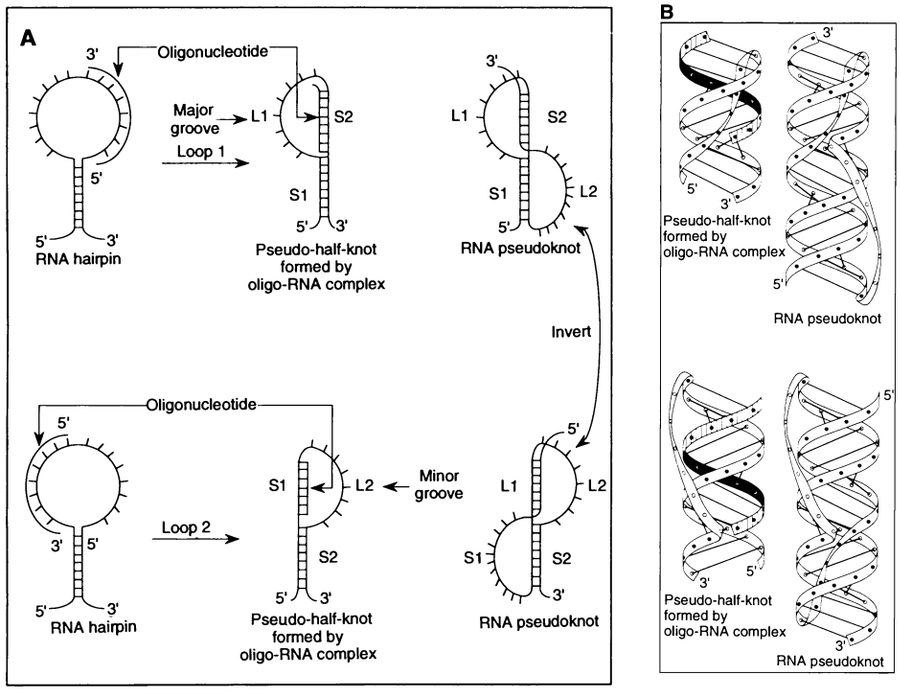

Fig. 1. The topology of pseudo–half-knots. (**A**) According to convention (*9*) the stems (S1 and S2) and loops (L1 and L2) are numbered consecutively from the 5′ end. Binding an oligonucleotide to the 3′ side (top path) or 5′ side (bottom path) of an RNA hairpin yields structures topologically similar to different halves of a pseudoknot with two coaxially stacked stems and a single loop that crosses the major groove (top path) or minor groove (bottom path). (**B**) Ribbon drawings of L1 (top) and L2 (bottom) pseudo–half-knots and similarly oriented pseudoknots. The oligonucleotides are drawn with striped (outer) and black (inner) surfaces.

loop (Fig. 1A, bottom path), the structure is equivalent to S1 and L2. We call these two structures loop 1 (L1) or loop 2 (L2) pseudo–half-knots.

The human immunodeficiency virus TAR element is a structured RNA that binds a viral regulatory protein known as Tat. Binding of Tat to TAR RNA is a critical step in the viral life cycle; therefore, disruption of Tat binding will block viral replication (*5*, *10*, *11*). To evaluate pseudo–half-knotting as an antisense design strategy, we targeted five sites on the TAR stem loop with RNA oligonucleotides. The 12-base oligonucleotides L1-12 and L2-12 target the 3′ and 5′ sides, respectively, of a hypothetical 17-base hairpin loop created by disrupting the four base pairs above the bulge in the TAR element (Fig. 2). We also designed three 17-base oligonucleotides: L1-17, which was targeted to form a loop 1 pseudo–half-knot; L2-17, which was targeted to form a loop 2 pseudo–half-knot; and ATWA-17, which was targeted to bind all the way around the 17-base hairpin without forming a pseudo–half-knot or disrupting base pairs below the bulge in the TAR stem (Table 1).

Structures of the five hybrid complexes were characterized by enzymatic and chemical probes (Figs. 2 and 3). Enzyme cleavage patterns consistent with the proposed pseudo–half-knot structures were obtained from

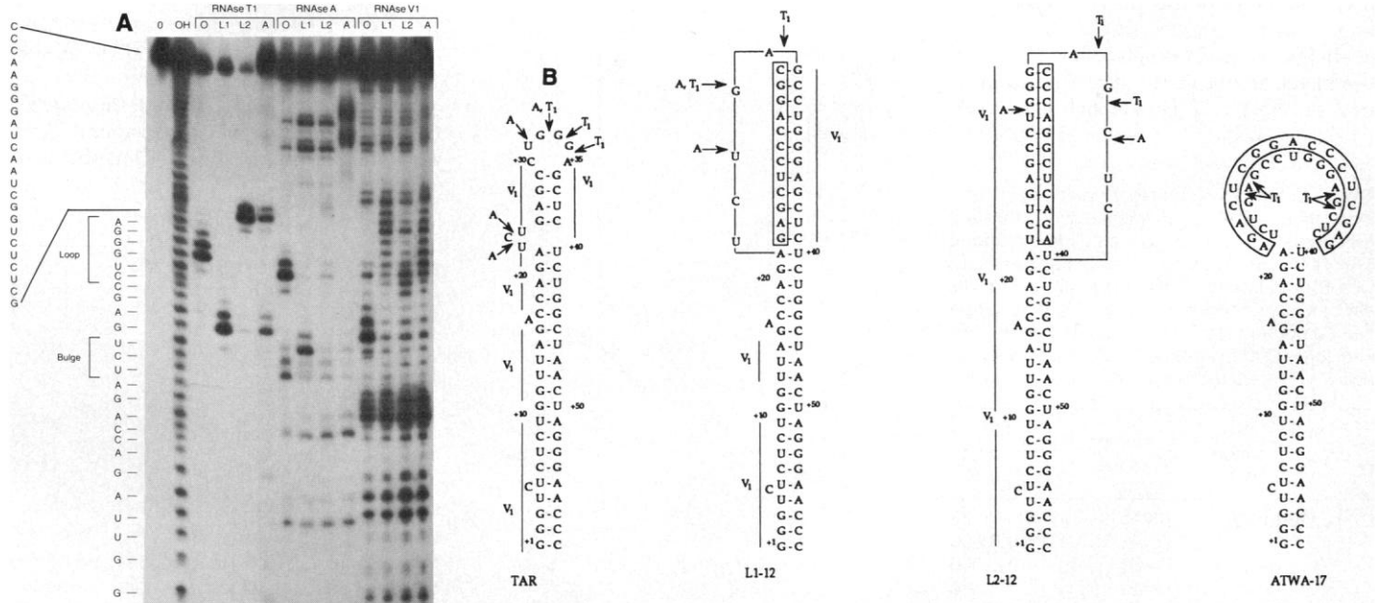

Fig. 2. (**A**) Enzymatic cleavage pattern in pseudo–half-knotted TAR RNA. TAR (100 pM) was hybridized with 100 nM L1-12 (L1), 100 nM L2-12 (L2), 1 mM ATWA (A), or no (O) oligonucleotides for 30 min at 37°C in 50 mM NaCl, 5 mM $MgCl_2$, 10 mM tris (pH 7.4) and then incubated with nuclease. RNase (ribonuclease) T1 and A cleave, respectively, at single-stranded G's or pyrimidines; RNase V1 cleaves double-stranded regions. (**B**) Sites of nuclease cleavage on TAR. Only the T1 cleavages are shown on the ATWA-17 complex (see text).

structures formed with both the 12-base (Fig. 2) and 17-base (*12*) oligonucleotides. The loop and bulge regions of TAR that were sensitive to the single-strand–specific nucleases T1 and A became protected upon oligonucleotide binding. The predicted single-stranded regions in the pseudo–half-knot became sensitive to T1 and A and lost sensitivity to double-strand–specific ribonuclease (RNase) V1.

The cleavage pattern obtained from the complex formed with the ATWA-17 oligonucleotide suggests that a pseudo–half-knot structure with only 12 of the 17 possible pairs was formed. If all 17 residues were paired in a pseudo–half-knot structure, some of the TAR stem below the bulge would be disrupted, but there was no evidence of this from the enzymatic cleavage patterns. The cleavage pattern suggests that oligonucleotide ATWA-17 bound to TAR is a mixed population of 12 base-paired L1 and L2 pseudo–half-knots, with the five remaining bases of the oligonucleotide dangling from either end of the heteroduplex.

The structure of the L1-17 pseudo–half-knot was further characterized by cleavage with orthophenanthroline-copper (OP•Cu) tethered to the 5′ end of the L1-17 oligonucleotide (*13*). Binding affinity and enzyme cleavage patterns for OP•Cu–L1-17 and untethered L1-17 oligonucleotides were identical, suggesting the OP moiety does not perturb the L1-17 pseudo–half-knot structure. Models of the L1-17 pseudo–half-knot structure place the OP•Cu in the major groove at the three-strand junction of the L1-17 pseudo–half-knot (Fig. 3B). Upon addition of the reducing agent to initiate OP•Cu cleavage, two predominant cuts in TAR were observed at C-19 and U-42. The cleavage site at C-19 is 21 bases away from the OP•Cu in the linear sequence (Fig. 3C), but in the pseudo–half-knot (Fig. 3B) it is adjacent to OP•Cu, consistent with the proposed structure.

Pseudo–half-knot formation disrupts the structure of TAR in the region specifically recognized by the Tat protein. Peptide fragments of Tat containing the TAR binding domain have been shown to bind specifically to the bulge region of TAR; this binding affinity is about 20-fold greater than that for the second and third binding sites on TAR (*14*). A 25–amino acid Tat fragment (residues 48 to 72 from the Tat protein), Tat-25, when bound to the TAR element in 1:1 stoichiometry, migrated on a native polyacrylamide gel at a location distinct from both uncomplexed TAR and TAR bound in a pseudo–half-knot (Fig. 4). Enzymatic mapping showed that under these conditions the peptide was bound at the bulge region (*12*).

To determine if the oligonucleotides could displace Tat-25 from TAR, we incubated ^{32}P-labeled TAR with either Tat-25 or the L1-12 oligonucleotide or with both. At peptide concentrations at which the 1:1 Tat-25:TAR complex predominated, the oligonucleotide completely displaced the Tat peptide (Fig. 4, lane 4). At higher peptide concentrations, second-site (non-bulge) binding occurred, and the pseudo–half-knot complex was shifted to a higher location on the gel (Fig. 4, lane 6) with the oligonucleotide remaining attached. Identical results were obtained with the L2-12 oligonucleotide (*12*) and were independent of the order of addition. These results further confirm that L1-12 and L2-12 bind to and disrupt the Tat binding site on TAR.

Drug design is facilitated if the affinity of the drug for the target site can be optimized. Experimental measurement of binding affinity determined by gel shift analysis (*15*) showed that the four L1 and L2 pseudo–half-knotting oligonucleotides bound TAR with high affinities (Table 1). The 17-base pseudo–half-knotting oligonucleotides bound TAR more strongly than the 12-base oligonucleotides. This stronger binding is not directly due to the additional base pairs in the 17-base oligonucleotides. Longer oligonucleotides are not necessarily more efficient at binding because the affinity gained from increasing the number of bases bound to the target is counteracted by unfavorable disruption of base pairs in the target. ATWA-17, the 17-base oligonucleotide that binds the TAR loop all the way around without pseudo–half-knotting, was the weakest binder, which is consistent with the notion that binding all the way around a loop is sterically not possible. However, shifting the oligonucleotide just three bases to the left or right on the target site to create the L2-17 or L1-17 compounds, respectively, increased the binding affinities 30- to 70-fold (Table 1).

The chemical composition of the oligonucleotides is an essential consideration. Oligonucleotides synthesized as 2′-*O*-methyl ana-

Table 1. Effect of chemical composition and loop structure on K_d's [dissociation constant (binding affinity)] for oligonucleotide binding to TAR RNA. Binding was done in 100 mM NaCl with 5′ end-labeled TAR and analyzed by gel shift as described previously (*15*). The target site numbering for TAR is indicated in Fig. 2B. The term *O*-Me refers to 2′-*O*-methyl analogs and P=S refers to phosphorothioate analogs.

Antisense oligonucleotide (target site)	Composition	TAR binding K_d (nM)
L1-12 (28 to 39)	RNA	75
	DNA	>100,000
	P=S	>100,000
	O-Me	70
L2-12 (23 to 34)	RNA	60
	O-Me	30
ATWA-17 (23 to 39)	RNA	500
L1-17 (26 to 42)	RNA	25
	DNA	>100,000
	O-Me	18
	P=S, *O*-Me	200
L2-17 (20 to 36)	RNA	15
	DNA	>100,000
	O-Me	7
	P=S, *O*-Me	150

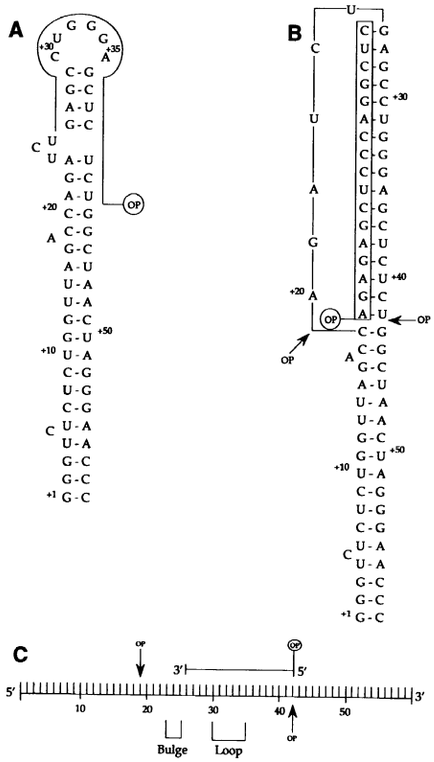

Fig. 3. L1-17–OP•Cu superimposed on the unperturbed TAR structure (**A**), the L1-17 pseudo–half-knot (**B**), and linear TAR (**C**). Sites of OP•Cu cleavage (arrows) are at C-19 and U-42.

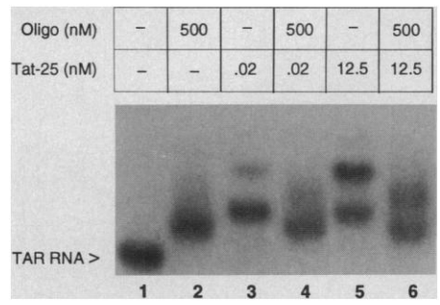

Fig. 4. Inhibition of Tat peptide binding by pseudo–half-knot oligonucleotides. N-acetylated Tat-25 used was obtained from the University of California at San Francisco Biotechnology Resource Core facility. Gel mobility shift assays were performed by the addition of 5′ ^{32}P TAR RNA and Tat-25 at indicated concentrations to a 10-μl reaction containing 10 mM tris-HCl (pH 7.5), 70 mM NaCl, 0.2 mM EDTA, 5% (v/v) glycerol, 500 nM bovine serum albumin, and 40 ng of polydIdC. Each binding mix was incubated for 30 min at 4°C and loaded directly onto a 15% native polyacrylamide gel.

logs had binding affinities similar to those of the RNA oligonucleotides (Table 1), consistent with the notion that 2′-O-methyl:RNA hybrids have affinities and geometries similar to RNA:RNA duplexes (*16*). The binding affinity of 2′-O-methyl phosphorothioate oligonucleotides for TAR was approximately ten times lower than that of 2′-O-methyl phosphodiesters. DNA and phosphorothioate analogs showed no detectable binding to the 12-base oligonucleotides and very slight binding to the 17-base oligonucleotides. This may be because the structure of DNA:RNA hybrids is different from that of RNA:RNA duplexes and because pseudo–half-knotting geometries appropriate for A-form helices are not optimal for DNA:RNA complexes. In addition, 2′-deoxyoligonucleotides hybridize to RNA much less tightly than do RNA (*17*) or 2′-O-methyl analogs.

Although considerable efforts are being directed at targeting RNA for therapeutic purposes, target site selection is still largely an empirical process. Analysis of the RNA target structure and bound complex stability and structure can assist in the design and optimization of functional antisense oligonucleotides (*18, 19*). By selection of relatively simple, short RNA structures, such as hairpin loops, and by binding with appropriately designed oligonucleotides, stable pseudo–half-knot structures can be formed.

Knowledge of the structure of a drug-target complex can also facilitate additional improvement in drug design. For example, results of the OP•Cu experiment could be used to design oligonucleotides to specifically cleave TAR near C-19. Moreover, these data demonstrate approaches to create nuclease-stable oligonucleotides that bind RNA with high affinity.

REFERENCES

1. Y. Eguchi, T. Itoh, J. Tomizawa, *Annu. Rev. Biochem.* **60**, 631 (1991).
2. G. W. Witherell, H.-N. Wu, O. C. Uhlenbeck, *Biochemistry* **29**, 11051 (1990).
3. J. L. Casey *et al.*, *Science* **240**, 924 (1988).
4. M. Junker-Niepmann, R. Bartenschlager, H. Schaller, *EMBO J.* **9**, 3389 (1990).
5. C. A. Rosen, G. N. Pavlakis, *AIDS* **4**, 499 (1990).
6. C. W. A. Pleij, *Trends Biochem. Sci.* **15**, 143 (1990).
7. C. W. Pleij and L. Bosch, *Methods Enzymol.* **180**, 289 (1989).
8. J. D. Puglisi, J. R. Wyatt, I. Tinoco, Jr., *Acc. Chem. Res.* **24**, 152 (1991).
9. C. W. Pleij, K. Rietveld, L. Bosch, *Nucleic Acids Res.* **13**, 1717 (1985).
10. S. Roy, U. Delling, C.-H. Chen, C. A. Rosen, N. Sonenberg, *Genes Dev.* **4**, 1365 (1990).
11. C. Dingwall *et al.*, *Proc. Natl. Acad. Sci. U.S.A.* **86**, 6925 (1989).
12. D. J. Ecker, unpublished material.
13. C. B. Chen and D. S. Sigman, *J. Am. Chem. Soc.* **110**, 6570 (1988).
14. K. M. Weeks, C. Ampe, S. C. Schultz, T. A. Steitz, D. M. Crothers, *Science* **249**, 1281 (1990).
15. A. M. Pyle, J. A. McSwiggen, T. R. Cech, *Proc. Natl. Acad. Sci. U.S.A.* **87**, 8187 (1990).
16. H. Inoue *et al.*, *Nucleic Acids Res.* **15**, 6131 (1987).
17. K. B. Hall and L. W. McLaughlin, *Biochemistry* **30**, 10606 (1991).
18. D. Ecker, in *Antisense Research and Applications*, S. Crooke and B. Lebleu, Eds., in preparation.
19. S. T. Crooke, *Annu. Rev. Pharmacol. Toxicol.* **32**, 329 (1992).

20. The authors acknowledge D. Sigman for the gift of 5-iodoacetamido-1,10-phenanthroline; R. Cedergren for the RNase program; I. Tinoco for introducing us to pseudoknots; and S. Crooke, J. Wyatt, O. Uhlenbeck, and I. Tinoco for helpful discussions and for critically reviewing this manuscript.

Combining Experimental Information from Crystal and Solution Studies: Joint X-ray and NMR Refinement

Boaz Shaanan,* Angela M. Gronenborn, Gerson H. Cohen, Gary L. Gilliland, B. Veerapandian, David R. Davies, G. Marius Clore

Joint refinement of macromolecules against crystallographic and nuclear magnetic resonance (NMR) observations is presented as a way of combining experimental information from the two methods. The model of interleukin-1β derived by the joint x-ray and NMR refinement is shown to be consistent with the experimental observations of both methods and to have crystallographic *R* value and geometrical parameters that are of the same quality as or better than those of models obtained by conventional crystallographic studies. The few NMR observations that are violated by the model serve as an indicator for genuine differences between the crystal and solution structures. The joint x-ray–NMR refinement can resolve structural ambiguities encountered in studies of multidomain proteins, in which low- to medium-resolution diffraction data can be complemented by higher resolution NMR data obtained for the individual domains.

With the emergence of NMR as a technique for determining the three-dimensional structure of proteins alongside crystallography (*1*), combination of experimental data from both methods opens a new avenue for the elucidation of macromolecular structures. A potential major hurdle in implementing such an approach, however, has been the apparent discrepancy between models derived by the two methods. Typically, the root-mean-square (rms) differences between backbone atoms of structures determined by the two methods are ~1.0 Å, with local differences of up to 2.0 Å or more (*2, 3*). Moreover, models obtained from crystallographic studies are frequently incompatible with the NMR data, as manifested in a relatively large number of nuclear Overhauser effect (NOE) violations; conversely, models obtained by NMR procedures tend to fit the x-ray data poorly (*R* values of 0.40 to 0.50). In this report we present a joint x-ray–NMR refinement and demonstrate that crystallographic and NMR data can be combined to produce models that are compatible with both experimental methods in that they have a minimal number of NOE violations and *R* values comparable to those derived from refinement against the crystallographic data alone. Further, the residual NOE violations in the combined model can serve as a reliable measure of genuine differences between the solution and crystal structures. A likely application of the method would be, for example, in the determination of structures of multidomain proteins.

The discrepancies between models derived from crystallographic and NMR methods are generally ascribed to distortions caused by crystal forces and differences in the media in which the two experiments are performed (*2, 3*). However, because both methods produce models through procedures that aim to satisfy the experimental data available to each technique and, at the same time, sets of stereochemical restraints (*4, 5*), the differences between the models may equally well be a reflection of inconsistencies between the computational procedures rather than that of genuine variations emanating from different molecular environments in the two experiments. The X-PLOR suite (*6*) provides a natural framework for testing this hypothesis. The structure selected as a test case was that of interleukin-1β (IL-1β), for which high-resolution NMR (*7*) and crystal structures (*8–10*) have been reported.

B. Shaanan, A. M. Gronenborn, G. H. Cohen, D. R. Davies, G. M. Clore, Laboratories of Molecular Biology and Chemical Physics, National Institute of Diabetes and Digestive and Kidney Diseases, National Institutes of Health, Building 2, Bethesda, MD 20892.
G. L. Gilliland and B. Veerapandian, Center for Advanced Research in Biotechnology of the Maryland Biotechnology Institute, University of Maryland, Shady Grove, and the National Institute of Standards and Technology, Rockville, MD 20850.

*Present address: Department of Biological Chemistry, The Hebrew University of Jerusalem, Jerusalem 91904, Israel.